Mon. Not. R. Astron. Soc. **380,** 78–92 (2007) doi:10.1111/j.1365-2966.2007.12051.x

Prompt emission of high-energy photons from gamma ray bursts

Nayantara Gupta★ and Bing Zhang★
Department of Physics and Astronomy, University of Nevada Las Vegas, Las Vegas, NV 89154, USA

Accepted 2007 May 25; Received 2007 May 23; in original form 2007 April 10

ABSTRACT

Within the internal shock scenario, we consider different mechanisms of high-energy (>1 MeV) photon production inside a gamma ray burst (GRB) fireball and derive the expected high-energy photon spectra from individual GRBs during the prompt phase. The photon spectra of leptonic and hadronic origins are compared within different sets of parameter regimes. Our results suggest that the high-energy emission is dominated by the leptonic component if the fraction of shock energy carried by electrons is not very small (e.g. $\epsilon_e > 10^{-3}$). For very small values of ϵ_e, the hadronic emission component could be comparable to or even exceed the leptonic component in the GeV–TeV regime. However, in this case a much larger energy budget of the fireball is required to account for the same level of the observed sub-MeV spectrum. The fireballs are therefore extremely inefficient in radiation. For a canonical fireball bulk Lorentz factor (e.g. $\Gamma = 400$), emissions above ∼10 GeV are attenuated by two-photon pair production processes. For a fireball with an even higher Lorentz factor, the cut-off energy is higher, and emissions of 10 TeV–PeV due to π^0-decay can also escape from the internal shocks. The flux level is, however, too low to be detected by current TeV detectors, and these photons also suffer attenuation by external soft photons. The GLAST Large Area Telescope can detect prompt emission of bright long GRBs above 100 MeV. For short GRBs, the prompt emission can be only barely detected for nearby bright ones with relatively 'long' durations (e.g. ∼1 s). With the observed high-energy spectrum alone, it appears that there is no clean picture to test the leptonic versus hadronic origin of the gamma rays. Such an issue may be, however, addressed by collecting both prompt and afterglow data. A moderate-to-high radiative efficiency would suggest a leptonic origin of high-energy photons, while a GRB with an extremely low radiative efficiency but an extended high-energy emission component would be consistent with (but not a proof for) the hadronic origin.

Key words: gamma-rays: bursts.

1 INTRODUCTION

The study of gamma ray bursts (GRBs) has been one of the most interesting areas in astrophysics in the past few years. Ongoing observational and theoretical investigations are disclosing the physical origin, characteristics of these objects as well as bringing new puzzles to us. EGRET detected high-energy photons from five GRBs coincident with triggers from the BATSE instrument (Jones et al. 1996). GRB 940217 was detected by EGRET independent of BATSE trigger, which has extended emission and with the highest energy photon of 18 GeV (Hurley et al. 1994). Gonzalez et al. (2003) discovered a distinct high-energy component up to 200 MeV in GRB 941017 that has a different temporal evolution with respect to the low-energy component. Although even higher energy gamma rays/neutrinos have not been firmly detected from GRBs yet, Atkins et al. (2000) have provided tentative evidence of TeV emission from GRB 970417A. For a long time, GRBs have been identified as potential sources of ultrahigh-energy cosmic rays (Waxman 1995; Vietri 1997). Within the standard fireball picture (e.g. Mészáros 2006), there are about a dozen mechanisms that can produce GeV–TeV gamma rays from GRBs (e.g. Zhang et al. 2007). More theoretical and observational efforts are needed to fully understand high-energy emission from GRBs. From the theoretical aspect, it is essential to investigate the relative importance of various emission components to identify the dominant mechanisms under certain conditions.

The high-energy photon spectra expected from GRBs during the prompt and the afterglow phases have been derived by various groups. In the scenario of external shock model the high-energy photon spectra during the early afterglow phase due to synchrotron and synchrotron self-Compton (SSC) emission by shock-accelerated relativistic electrons and protons have been studied (Mészáros, Rees & Papathanassiou

★E-mail: nayan@physics.unlv.edu (NG); bzhang@physics.unlv.edu (BZ)

1994; Mészáros & Rees 1994; Panaitescu & Mészáros 1998; Totani 1998; Wei & Lu 1998; Chiang & Dermer 1999; Dermer, Bottcher & Chiang 2000a; Dermer, Chiang & Mitman 2000b; Panaitescu & Kumar 2000; Sari & Esin 2001; Zhang & Mészáros 2001; Fan et al. 2007; Gou & Mészáros 2007). In the case of a strong reverse shock emission component, the SSC emission in the reverse shock region or the crossing inverse-Compton (IC) processes between the forward and reverse shock regions are also important (Wang, Dai & Lu 2001a,b; Pe'er & Waxman 2005). The discovery of X-ray flares in early afterglows in the *Swift* era (Burrows et al. 2005) also opens the possibility that scattering of the flaring photons from the external shocks can give strong GeV emission (Fan & Piran 2006; Wang, Li & Mészáros 2006). The effect of cosmic infrared background on high-energy delayed gamma rays from GRBs has been also widely discussed in the literature (Dai & Lu 2002; Stecker 2003; Razzaque, Mészáros & Zhang 2004; Wang et al. 2004; Casanova, Dingus & Zhang 2007; Murase, Asano & Nagataki 2007). The most important high-energy emission component is believed to be emitted from the prompt phase. *Swift* early X-ray afterglow data suggest that the GRB prompt emission is of 'internal' origin, unlike the external-origin afterglow emission (Zhang et al. 2006, cf. Dermer 2007). The most widely discussed internal model of prompt emission is the internal shock model (Rees & Mészáros 1994). Within the internal shock model the spectrum of high-energy photons expected during the prompt phase has been studied (Pilla & Loeb 1998; Bhattacharjee & Gupta 2003; Fragile et al. 2004; Pe'er & Waxman 2004; Razzaque et al. 2004; Pe'er, Mészáros & Rees 2006). The various processes of high-energy photon production in the internal shocks are electron synchrotron emission, SSC of electrons, synchrotron emission of protons, photon production through π^0 decay produced in proton–photon (p–γ) interactions and radiations by secondary positrons produced from π^+ decays. In this paper, we consider all these processes self-consistently with a semi-analytical approach and study the relative importance of each component within the internal shock scenario. The derived photon spectra are corrected for internal optical depth for pair production, which is energy-dependent and also depends on various other parameters of GRBs, for example, their variability times, luminosities, the low-energy photon spectra inside GRBs, and photon spectral break energies. If the electrons cool down by synchrotron and SSC emission to trans-relativistic energies, then they accumulate near a value of Lorentz factor of around unity. The accumulated electrons affect the high-energy photon spectrum by direct-Compton scattering and other processes, which make the spectrum significantly different from the broken power laws considered in this work, see (Pe'er, Mészáros & Rees 2005; Pe'er et al. 2006) for detailed discussions. In any case, for the values of parameters considered in the present paper this effect is not significant.

GLAST's (Gehrels & Michelson 1999) burst monitor (GBM) will detect photons in the energy range of 10 keV–25 MeV and Large Area Telescope (LAT) will detect photons in the energy range of 20 MeV–1000 GeV. With a large field of view (>2 sr for LAT), GLAST will detect high-energy photons from many GRBs and open a new era of studying GRBs in the high-energy regime. This is supplemented by AGILE (Longo, Cocco & Tavani 2002), which is designed to observe photons in the energy range of 10–40 keV and 30 MeV–50 GeV and also has a large field of view. There are several other ground-based detectors, for example, Whipple/VERITAS (Horan et al. 2007), Milagro (Atkins et al. 2004), which have been searching or will search for ∼TeV photons from GRBs. Detections or non-detections of high-energy gamma rays from GRBs with space-based and ground-based detectors in the near future would make major steps in revealing the physical environment, bulk motion, mechanisms of particle acceleration and high-energy photon production, photon densities, etc., of GRBs.

2 ELECTRON SYNCHROTRON RADIATION

We define the following three reference frames. (i) The comoving frame or the wind rest frame is the rest frame of the outflowing ejecta expanding with a Lorentz factor Γ with respect to the observer and the central engine; (ii) the source rest frame is attached to the GRB central engine at a redshift z; and (iii) the observer's frame is the reference frame of the observer on earth, which is related to the source rest frame by the redshift correction factor. We denote the quantities measured in the comoving frame with primes. The shock-accelerated relativistic electrons lose energy by synchrotron radiation and SSC in the shock region. Assuming a power-law distribution of fresh electrons accelerated from the internal shocks and considering a continuous injection of electrons during the propagation of the shocks, the relativistic primary electron number distribution in the comoving frame can be expressed as a broken power law in energy: (Sari, Piran & Narayan 1998):

$$\frac{\mathrm{d}N_{\mathrm{e}}(E'_{\mathrm{e}})}{\mathrm{d}E'_{\mathrm{e}}} \propto \begin{cases} E'^{-p}_{\mathrm{e}} & E'_{\mathrm{e,m}} < E'_{\mathrm{e}} < E'_{\mathrm{e,c}} \\ E'^{-p-1}_{\mathrm{e}} & E'_{\mathrm{e,c}} < E'_{\mathrm{e}} \end{cases} \tag{1}$$

in the case of slow cooling, where $E'_{\mathrm{e,m}}$ is the minimum injection energy of electrons and $E'_{\mathrm{e,c}}$ is the energy of an electron that loses its energy significantly during the dynamic time-scale, known as the cooling energy of the electrons. If the electrons are cooling fast so that even the electrons with the minimum injection energy have cooled during the dynamical time-scale, by considering continuous injection of electrons from the shock the comoving electron number distribution can be expressed as

$$\frac{\mathrm{d}N_{\mathrm{e}}(E'_{\mathrm{e}})}{\mathrm{d}E'_{\mathrm{e}}} \propto \begin{cases} E'^{-2}_{\mathrm{e}} & E'_{\mathrm{e,c}} < E'_{\mathrm{e}} < E'_{\mathrm{e,m}} \\ E'^{-p-1}_{\mathrm{e}} & E'_{\mathrm{e,m}} < E'_{\mathrm{e}} \end{cases} . \tag{2}$$

If the electrons cool down to subrelativistic energies, then they accumulate near electron Lorentz factor $\gamma'_{\mathrm{e}} \sim 1$. This effect may distort the high-energy photon spectrum by direct-Compton scattering (Pe'er et al. 2005, 2006), and we focus on the parameter regime where this effect is not significant. The energies in the source rest frame and the comoving frame are related as $E_{\mathrm{e}} \simeq \Gamma E'_{\mathrm{e}}$, where Γ is the average bulk Lorentz factor of the GRB fireball in the prompt phase. The expression for the minimum injection energy of electrons in the comoving frame is $E'_{\mathrm{e,m}} = m_{\mathrm{e}}c^2\bar{\gamma}'_{\mathrm{p}}g(p)\frac{m_{\mathrm{p}}}{m_{\mathrm{e}}}\frac{\epsilon_{\mathrm{e}}}{\epsilon_{\mathrm{p}}}$, where $g(p) = \frac{p-2}{p-1}$ for $p \gg 2$ and $g(p) \sim 1/6$ for $p = 2$ (Razzaque & Zhang 2007), m_{p} and m_{e} are the masses of proton and electron, respectively, and $\bar{\gamma}'_{\mathrm{p}}m_{\mathrm{p}}c^2$ is the average internal energy of protons in the comoving frame. We have assumed $\bar{\gamma}'_{\mathrm{p}}$ to be

of the order of unity (in principle $\bar{\gamma}'_{\rm p}$ could be smaller than unity). The total internal energy is distributed among electrons, protons and the internal magnetic fields within the internal shocks. The fractions of the total energy carried by electrons, protons and internal magnetic fields are represented by $\epsilon_{\rm e}$, $\epsilon_{\rm p}$ and ϵ_B, respectively, where $\epsilon_{\rm e}+\epsilon_{\rm p}+\epsilon_B=1$. We have assumed that all the electrons and protons are accelerated in internal shocks. In reality, the shock-accelerated particles may be only a fraction of the total population and additional fractional parameters ($\xi_{\rm e}$, $\xi_{\rm p}$) may be introduced (e.g. Bykov & Mészáros 1996). In such a case, the following treatments are still generally valid by re-defining $\epsilon'_{\rm e}=\epsilon_{\rm e}/\xi_{\rm e}$ and $\epsilon'_{\rm p}=\epsilon_{\rm p}/\xi_{\rm p}$, while the relation $\epsilon_{\rm e}+\epsilon_{\rm p}+\epsilon_B=1$ still holds.

The relativistic electrons lose their energy by synchrotron radiation and IC scattering (Panaitescu & Mészáros 1998; Sari & Esin 2001; Zhang & Mészáros 2001). The comoving cooling break energy in the relativistic electron spectrum can be derived by comparing the cooling and the dynamical time-scales. The comoving cooling time-scale $t'_{\rm cool}$ of electrons is a convolution of the cooling time-scales for synchrotron radiation $t'_{\rm syn}$ and for IC scattering $t'_{\rm IC}$:

$$\frac{1}{t'_{\rm cool}}=\frac{1}{t'_{\rm syn}}+\frac{1}{t'_{\rm IC}}. \tag{3}$$

We denote U as the internal energy density of the internal shock, and $U_{\rm e}$ and U_B as the energy densities of electrons and magnetic fields, respectively. The energy density of the synchrotron radiation is $U_{\rm e,syn}=\frac{\eta_{\rm e}U_{\rm e}}{1+Y_{\rm e}}=\frac{\eta_{\rm e}\epsilon_{\rm e}U}{1+Y_{\rm e}}$ (Sari & Esin 2001), where the radiation efficiency of electrons is $\eta_{\rm e}=[(E'_{\rm e,c}/E'_{\rm e,m})^{2-p},\,1]$ for slow and fast cooling, respectively, and

$$Y_{\rm e}=\frac{L_{\rm e,IC}}{L_{\rm e,syn}}=\frac{U_{\rm e,syn}}{U_B}=\frac{-1+\sqrt{1+4\eta_{\rm e}\epsilon_{\rm e}/\epsilon_B}}{2} \tag{4}$$

denotes the relative importance between the IC and the synchrotron emission components.[1] $L_{\rm e,IC}$ and $L_{\rm e,syn}$ are the luminosities of radiations emitted in SSC and synchrotron emission of relativistic electrons, respectively. The inverse of the cooling time-scale of electrons can be expressed by the power divided by energy ($E'_{\rm e}=m_{\rm e}\gamma'_{\rm e}c^2$),

$$\frac{1}{t'_{\rm cool}}=\frac{4}{3}\sigma_{\rm e,T}\beta_{\rm e}^{'2}\gamma'_{\rm e}\frac{c}{m_{\rm e}c^2}(U_B+U_{\rm e,syn})=\frac{4}{3}\sigma_{\rm e,T}\beta_{\rm e}^{'2}\gamma'_{\rm e}\frac{cU\epsilon_B}{m_{\rm e}c^2}(1+Y_{\rm e}), \tag{5}$$

where $\sigma_{\rm e,T}$ is Thomson cross-section of electrons, $\beta'_{\rm e}\simeq 1$ is the dimensionless speed of the relativistic electrons. The comoving dynamical time-scale is $t'_{\rm dyn}\simeq\Gamma t_{\rm v}$, where Γ is the average Lorentz factor of the GRB, and $t_{\rm v}$ is the variability time in the source rest frame of the GRB, which denotes the variability time-scale of the central engine. Throughout the paper, we assume that electron synchrotron radiation from the internal shocks is the mechanism that power the prompt gamma-ray emission in the sub-MeV band. However, for standard parameters within this scenario the cooling time-scale of electrons is much shorter than the dynamical time-scale of GRBs. As a result the flux density $[E_{\gamma,{\rm s}}\frac{{\rm d}N_{\gamma,{\rm s}}(E_{\gamma,{\rm s}})}{E_{\gamma,{\rm s}}}]$ below the cooling break energy is proportional to $E_{\gamma,{\rm s}}^{-1/2}$ and cannot explain the harder spectral indices observed in many GRBs (Ghisellini, Celotti & Lazzati 2000). If the magnetic field created by internal shocks decays on a length-scale much shorter then the comoving width of the plasma, then the resulting synchrotron radiation can explain some of the broadband GRB spectra observed by *Swift* (Pe'er & Zhang 2006). In this case the effective dynamical time-scale is shorter by a factor of $f_{\rm c}$ than its actual value. Hence, the ratio of the cooling and the dynamical time-scale can be expressed as

$$\frac{t'_{\rm dyn}}{t'_{\rm cool}}=f_{\rm c} \tag{6}$$

at the cooling energy $E'_{\rm e}=E'_{\rm e,c}$. The expression of the electron cooling energy in the comoving frame can be written as

$$E'_{\rm e,c}=\gamma'_{\rm e,c}m_{\rm e}c^2=m_{\rm e}c^2\frac{3m_{\rm e}c^2f_{\rm c}}{4\Gamma t_{\rm v}\sigma_{\rm e,T}cU\epsilon_B(1+Y_{\rm e})}=530\ {\rm keV}\frac{t_{\rm v,-2}\Gamma_2^5f_{c,2}}{L_{\rm iso,51}\epsilon_{B,-1}(1+Y_{\rm e})}. \tag{7}$$

Here and throughout the text the convention $Q_x=Q/10^x$ is adopted in cgs units. In the above expression $L_{\rm iso}$ is the luminosity corresponding to the energy $E_{\rm iso}$ carried by all particles and the magnetic fields in the shocks. It is a fraction of the wind (outflow) luminosity $L_{\rm iso}\sim\eta L_{\rm w}$, where η is the efficiency of converting the kinetic energy of the wind to the shock internal energy. The luminosity $L_{\rm iso}$ and internal energy U are related as $U=L_{\rm iso}/(4\pi\Gamma^2r_{\rm is}{}^2c)$, where $r_{\rm is}=\Gamma^2ct_{\rm v}$ is the internal shock radius. The synchrotron spectrum is a multisegment broken power law (Sari et al. 1998) separated by several breaks, including the emission frequency from electrons with the minimum injection energy, the cooling break frequency, and the synchrotron self-absorption frequency (Rybicki & Lightman 1979). In the internal shocks, the magnetic field in the comoving frame can be expressed as (Zhang & Mészáros 2002):

$$B'\simeq 4.4\times10^5{\rm G}(\xi_1\epsilon_{B,-1})^{1/2}L_{\rm iso,51}^{1/2}r_{\rm is,13}^{-1}\Gamma_2^{-1}=1.5\times10^6{\rm G}\frac{(\xi_1\epsilon_{B,-1}L_{\rm iso,51})^{1/2}}{\Gamma_2^3t_{\rm v,-2}}, \tag{8}$$

where ξ is the compression ratio, which is about 7 for strong shocks. The synchrotron self-absorption energy ($E_{\rm ssa}$) in internal shocks can be expressed as (Li & Song 2004; Fan et al. 2005; cf. Pe'er & Waxman 2004):

$$E_{\rm ssa}\simeq 0.24\ {\rm keV}L_{\gamma,{\rm s},51}^{2/7}\Gamma_2^{3/7}r_{\rm is,13}^{-4/7}B_5'{}^{1/7}=0.69\ {\rm keV}L_{\rm iso,51}^{5/14}t_{\rm v,-2}^{-5/7}\Gamma_2{}^{-8/7}(\xi_1\epsilon_{B,-1})^{1/14}\left(\frac{\epsilon_{\rm e}\eta_{\rm e}}{1+Y_{\rm e}}\right)^{2/7}, \tag{9}$$

[1] Strictly speaking, such a treatment is valid for the IC process in the Thomson regime. However, this is also a reasonable approximation if the peak of the spectral energy distribution of the IC component is in the Thomson regime, which is generally the case for the calculations performed in this paper.

where $L_{\gamma,\rm s} = L_{\rm iso}\,\epsilon_{\rm e}\,\eta_{\rm e}/(1+Y_{\rm e})$ is the isotropic gamma-ray luminosity due to synchrotron radiation. The cooling break energy $E'_{\rm e,c}$ and the minimum injection energy $E'_{\rm e,m}$ of the electrons define two break energies in the synchrotron photon spectrum. The cooling break energy in the photon spectrum in the source rest frame is

$$E_{\gamma,\rm c} = \Gamma\frac{3h}{4\pi}\left[\frac{E'_{\rm e,c}}{m_{\rm e}c^2}\right]^2\frac{eB'c}{m_{\rm e}c^2} \simeq 1.9\times10^{-3}\ {\rm eV}\Gamma_2\left(\frac{t_{\rm v,-2}\Gamma_2^5 f_{c,2}}{L_{\rm iso,51}\epsilon_B(1+Y_{\rm e})}\right)^2 B'_5 = 2.8\,{\rm eV}t_{\rm v,-2}\frac{\xi_1^{1/2}}{(L_{\rm iso,51}\epsilon_{B,-1})^{3/2}}\left(\frac{\Gamma_2^4 f_{c,2}}{1+Y_{\rm e}}\right)^2. \quad (10)$$

Note that $E_{\gamma,\rm c}$ very sensitively depends on Γ and some other parameters so that it could become a large value when parameters change. For example, for $B' = 10^4$ G, $\Gamma = 400, f_{\rm c} = 500$, $L_{\rm iso} = 10^{51}$ erg s^{-1}, $t_{\rm v} = 0.01$ s and $\epsilon_B = 0.1$ we get $E_{\gamma,\rm c} \sim 1.9$ MeV. The break energy in the photon spectrum due to the minimum electron injection energy is

$$E_{\gamma,\rm m} = \Gamma\frac{3h}{4\pi}\left(\frac{E'_{\rm e,m}}{m_{\rm e}c^2}\right)^2\frac{eB'c}{m_{\rm e}c^2} \simeq 0.58\ {\rm MeV}\Gamma_2\left(\frac{\epsilon_{\rm e}}{\epsilon_{\rm p}}\right)^2 B'_5 = 8.5\,{\rm MeV}\left(\frac{\epsilon_{\rm e}}{\epsilon_{\rm p}}\right)^2(\xi_1\epsilon_{B,-1}L_{\rm iso,51})^{1/2}\left(\Gamma_2^2 t_{\rm v,-2}\right)^{-1}. \quad (11)$$

Assuming $E_{\rm ssa} < E_{\gamma,\rm m,s} < E_{\gamma,\rm c,s}$ the photon energy spectrum from synchrotron radiation of slow-cooling relativistic electrons is as follows:

$$E_{\gamma,\rm s}^2\frac{{\rm d}N_{\gamma,\rm s}(E_{\gamma,\rm s})}{{\rm d}E_{\gamma,\rm s}} \propto \begin{cases} E_{\gamma,\rm s}^{4/3} & E_{\rm ssa} < E_{\gamma,\rm s} \leqslant E_{\gamma,\rm m,s} \\ E_{\gamma,\rm m,s}^{4/3+(p-3)/2}E_{\gamma,\rm s}^{-(p-3)/2} & E_{\gamma,\rm m,s} < E_{\gamma,\rm s} \leqslant E_{\gamma,\rm c,s} \\ E_{\gamma,\rm m,s}^{4/3+(p-3)/2}E_{\gamma,\rm c,s}^{1/2}E_{\gamma,\rm s}^{-(p-2)/2} & E_{\gamma,\rm c,s} \leqslant E_{\gamma,\rm s} \end{cases}. \quad (12)$$

In the case of slow-cooling electrons for very small values of $\epsilon_{\rm e}$ (e.g. $\sim10^{-3}$, which is relevant when the hadronic emission component becomes important), the break in the photon spectrum due to the minimum injection energy of electrons goes below the synchrotron self-absorption energy. The order in the spectral break energies becomes $E_{\gamma,\rm m,s} < E_{\rm ssa} < E_{\gamma,\rm c,s}$, and the spectrum is also modified. The spectral indices of the electron synchrotron spectrum for different ordering of the spectral break energies are derived by Granot & Sari (2002). For $E_{\gamma,\rm m,s} < E_{\gamma,\rm s} < E_{\rm ssa}$, the spectral index of $E_{\gamma,\rm s}^2\frac{{\rm d}N_{\gamma,\rm s}(E_{\gamma,\rm s})}{{\rm d}E_{\gamma,\rm s}}$ is 7/2, and for $E_{\gamma,\rm s} < E_{\gamma,\rm m,s}$ the spectral index is 3. The indices of the spectrum between $E_{\rm ssa}$, $E_{\gamma,\rm c,s}$ and above $E_{\gamma,\rm c,s}$ remain as $-(p-3)/2$ and $-(p-2)/2$, respectively. When $E_{\rm ssa}$ is greater than both $E_{\gamma,\rm m,s}$ and $E_{\gamma,\rm c,s}$ their relative ordering becomes unimportant. In that case the spectral indices of $E_{\gamma,\rm s}^2\frac{{\rm d}N_{\gamma,\rm s}(E_{\gamma,\rm s})}{{\rm d}E_{\gamma,\rm s}}$ are 7/2 between $E_{\gamma,\rm m,s}$ and $E_{\rm ssa}$, and $-(p-2)/2$ above $E_{\rm ssa}$. Below $E_{\gamma,\rm m,s}$ the index is 3.

For fast-cooling electrons the synchrotron photon energy spectrum for $E_{\rm ssa} < E_{\gamma,\rm c,s} < E_{\gamma,\rm m,s}$ is

$$E_{\gamma,\rm s}^2\frac{{\rm d}N_{\gamma,\rm s}(E_{\gamma,\rm s})}{{\rm d}E_{\gamma,\rm s}} \propto \begin{cases} E_{\gamma,\rm s}^{4/3} & E_{\rm ssa} < E_{\gamma,\rm s} \leqslant E_{\gamma,\rm c,s} \\ E_{\gamma,\rm c,s}^{5/6}E_{\gamma,\rm s}^{1/2} & E_{\gamma,\rm c,s} < E_{\gamma,\rm s} \leqslant E_{\gamma,\rm m,s} \\ E_{\gamma,\rm c,s}^{5/6}E_{\gamma,\rm m,s}^{(p-1)/2}E_{\gamma,\rm s}^{-(p-2)/2} & E_{\gamma,\rm m,s} \leqslant E_{\gamma,\rm s} \end{cases}. \quad (13)$$

When the ordering of break energies in the photon spectrum becomes $E_{\gamma,\rm c,s} < E_{\rm ssa} < E_{\gamma,\rm m,s}$, the photon energy spectrum is

$$E_{\gamma,\rm s}^2\frac{{\rm d}N_{\gamma,\rm s}(E_{\gamma,\rm s})}{{\rm d}E_{\gamma,\rm s}} \propto \begin{cases} E_{\gamma,\rm s}^{13/8} & E_{\rm ssa} < E_{\gamma,\rm s} \leqslant E_{\gamma,\rm c,s} \\ E_{\gamma,\rm c,s}^{9/8}E_{\gamma,\rm s}^{1/2} & E_{\gamma,\rm c,s} < E_{\gamma,\rm s} \leqslant E_{\gamma,\rm m,s} \\ E_{\gamma,\rm c,s}^{9/8}E_{\gamma,\rm m,s}^{(p-1)/2}E_{\gamma,\rm s}^{-(p-2)/2} & E_{\gamma,\rm m,s} \leqslant E_{\gamma,\rm s} \end{cases}. \quad (14)$$

The total energy emitted in synchrotron radiation by relativistic electrons is $E_{\rm iso}\eta_{\rm e}\epsilon_{\rm e}/(1+Y_{\rm e})$. The normalization constant for the synchrotron photon energy spectrum can be calculated from

$$\int_{E_{\gamma,\rm min}}^{E_{\gamma,\rm max}} E_{\gamma,\rm s}\frac{{\rm d}N_{\gamma,\rm s}(E_{\gamma,\rm s})}{{\rm d}E_{\gamma,\rm s}}\,{\rm d}E_{\gamma,\rm s} = E_{\rm iso}\frac{\eta_{\rm e}\epsilon_{\rm e}}{(1+Y_{\rm e})}. \quad (15)$$

The maximum electron energy $E_{\rm e,max}$ can be calculated by equating the acceleration time and the shorter of the dynamical and cooling time-scales of the relativistic electrons. The expression of the acceleration time-scale is $t'_{\rm acc} = 2\pi\zeta\, r_{\rm L}(E'_{\rm e})/c = 2\pi\zeta\, E'_{\rm e}/eB'c$. Here $r_{\rm L}(E'_{\rm e})$ is the Larmor radius of an electron of energy $E'_{\rm e}$ in a magnetic field B', ζ can be expressed as $\zeta \sim {\beta_{\rm sh}}^{-2}y$, where $\beta_{\rm sh}$ is the velocity of the shock in the comoving frame of the unshocked medium and y is the ratio of diffusion coefficient to the Bohm coefficient Rachen & Mészáros (1998). In ultrarelativistic shocks $\beta_{\rm sh} \approx 1$ and numerical simulations for both parallel and oblique shocks gives $\zeta \sim 1$. With

$$t'_{\rm acc} = \min[t'_{\rm cool}, t'_{\rm dyn}], \quad (16)$$

one can derive the maximum comoving electron energy

$$E\prime_{\rm e,max} = \min\left[8.5\left(\frac{B'_5\Gamma_2^6 t_{\rm v,-2}^2}{L_{\rm iso,51}\epsilon_B(1+Y_{\rm e})}\right)^{1/2}, 14.3\times10^7\Gamma_2 t_{\rm v,-2}B'_5\right]{\rm GeV}. \quad (17)$$

For electrons, the cooling term (first term in the bracket) always defines the maximum electron energy. The maximum synchrotron photon energy in the source rest frame can be then derived as

$$E_{\gamma,\rm max} = \Gamma\frac{3h}{4\pi}\left(\frac{E'_{\rm e,max}}{m_{\rm e}c^2}\right)^2\frac{eB'c}{m_{\rm e}c^2} = 0.48\ {\rm GeV}\left(\frac{\Gamma_2^7 {B'_5}^2 t_{\rm v,-2}^2}{L_{\rm iso,51}\epsilon_{B,-1}(1+Y_{\rm e})}\right) = 102\ {\rm GeV}\left(\frac{\Gamma_2}{1+Y_{\rm e}}\right). \quad (18)$$

This is used in equation (15) to define the normalization of the spectrum. The result has a very steep dependence on Γ. We also note that B' is not an independent parameter, but can be calculated from other parameters according to equation (8). For example, for $\Gamma = 400$, $L_{\rm iso} =$

10^{51} erg s^{-1}, $t_{\rm v} = 0.01$ s and $\epsilon_B, \epsilon_{\rm e} \sim 0.1$, the magnetic field is of the order of 10^4 G and the maximum photon energy becomes a few hundred GeV.

3 ELECTRON INVERSE-COMPTON SCATTERING

The relativistic electrons can be IC scattered by low-energy synchrotron photons inside the GRB fireball and transfer their energy to high-energy photons. Below, we derive the IC photon spectrum using the electron and synchrotron photon spectra:

$$\frac{{\rm d}N_{\gamma,{\rm i}}(E_{\gamma,{\rm i}})}{{\rm d}E_{\gamma,{\rm i}}} \propto \frac{1}{E_{\gamma,{\rm i}}} \int \frac{{\rm d}N_{\rm e}(E_{\rm e})}{{\rm d}E_{\rm e}} {\rm d}E_{\rm e} \times \int \frac{{\rm d}N_{\gamma,{\rm s}}(E_{\gamma,{\rm s}})}{{\rm d}E_{\gamma,{\rm s}}} {\rm d}E_{\gamma,{\rm s}}. \tag{19}$$

The electron Lorentz factor ($\gamma'_{\rm e}$), IC and synchrotron photon energies ($E_{\gamma,{\rm i}}$, $E_{\gamma,{\rm s}}$) are related as $E_{\gamma,{\rm i}} \sim \gamma'^2_{\rm e} E_{\gamma,{\rm s}}$, this can be used to simplify the above equation. The final expression for the IC photon spectrum considering slow cooling of electrons is

$$E^2_{\gamma,{\rm i}} \frac{{\rm d}N_{\gamma,{\rm i}}(E_{\gamma,{\rm i}})}{{\rm d}E_{\gamma,{\rm i}}} \propto \begin{cases} E^{4/3}_{\gamma,{\rm i}} & E_{\rm ssa,i} < E_{\gamma,{\rm i}} \leqslant E_{\gamma,{\rm m,i}} \\ E^{4/3+(p-3)/2}_{\gamma,{\rm m,i}} E^{-(p-3)/2}_{\gamma,{\rm i}} & E_{\gamma,{\rm m,i}} < E_{\gamma,{\rm i}} \leqslant E_{\gamma,{\rm c,i}} \\ E^{4/3+(p-3)/2}_{\gamma,{\rm m,i}} E^{1/2}_{\gamma,{\rm c,i}} E^{-(p-2)/2}_{\gamma,{\rm i}} & E_{\gamma,{\rm c,i}} < E_{\gamma,{\rm i}} \leqslant E_{\gamma,{\rm K}} \\ E^{4/3+(p-3)/2}_{\gamma,{\rm m,i}} E^{1/2}_{\gamma,{\rm c,i}} E^{(p-2)/2}_{\gamma,{\rm K}} E^{-(p-2)}_{\gamma,{\rm i}} & E_{\gamma,{\rm K}} < E_{\gamma,{\rm i}} \end{cases}. \tag{20}$$

Here $E_{\rm ssa,i} = \gamma'^2_{\rm e,m} E_{\rm ssa}$, $E_{\gamma,{\rm m,i}} = \gamma'^2_{\rm e,m}\, E_{\gamma,{\rm m,s}}$, and $E_{\gamma,{\rm c,i}} = \gamma'^2_{\rm e,c} E_{\gamma,{\rm c,s}}$, where $\gamma'_{\rm e,m} = E'_{\rm e,m}/m_{\rm e}c^2 = g(p)(m_{\rm p}/m_{\rm e})(\epsilon_{\rm e}/\epsilon_{\rm p})$ and $\gamma'_{\rm e,c} = E'_{\rm e,c}/m_{\rm e}c^2$ are Lorentz factors corresponding to the minimum injection energy of electrons and the cooling break energy of electrons. In the case of fast cooling $E_{\gamma,{\rm m,i}} > E_{\gamma,{\rm c,i}}$ and the IC photon spectrum has to be modified accordingly:

$$E^2_{\gamma,{\rm i}} \frac{{\rm d}N_{\gamma,{\rm i}}(E_{\gamma,{\rm i}})}{{\rm d}E_{\gamma,{\rm i}}} \propto \begin{cases} E^{4/3}_{\gamma,{\rm i}} & E_{\rm ssa,i} < E_{\gamma,{\rm i}} \leqslant E_{\gamma,{\rm c,i}} \\ E^{5/6}_{\gamma,{\rm c,i}} E^{1/2}_{\gamma,{\rm i}} & E_{\gamma,{\rm c,i}} < E_{\gamma,{\rm i}} \leqslant E_{\gamma,{\rm m,i}} \\ E^{5/6}_{\gamma,{\rm c,i}} E^{(p-1)/2}_{\gamma,{\rm m,i}} E^{-(p-2)/2}_{\gamma,{\rm i}} & E_{\gamma,{\rm m,i}} < E_{\gamma,{\rm i}} \leqslant E_{\gamma,{\rm K}} \\ E^{5/6}_{\gamma,{\rm c,i}} E^{(p-1)/2}_{\gamma,{\rm m,i}} E^{(p-2)/2}_{\gamma,{\rm K}} E^{-(p-2)}_{\gamma,{\rm i}}, & E_{\gamma,{\rm K}} < E_{\gamma,{\rm i}} \end{cases}. \tag{21}$$

In equation (21), the expressions for $E_{\rm ssa,i}$, $E_{\gamma,{\rm c,i}}$ and $E_{\gamma,{\rm m,i}}$ are $E_{\rm ssa,i} = \gamma'^2_{\rm e,c} E_{\rm ssa}$, $E_{\gamma,{\rm c,i}} = \gamma'^2_{\rm e,c} E_{\gamma,{\rm c,s}}$ and $E_{\gamma,{\rm m,i}} = \gamma'^2_{\rm e,m} E_{\gamma,{\rm m,s}}$. When $E_{\rm e}E_{\gamma,{\rm s}} \gg \Gamma^2 m^2_{\rm e} c^4$ the cross-section for IC scattering decreases as the scattering enters the Klein–Nishina (KN) regime. A break in the photon spectrum at $E_{\gamma,{\rm i}} = E_{\gamma,{\rm K}}$ appears when the KN effect becomes important. We define a parameter $\kappa = \frac{E_{\rm e} E_{\gamma,{\rm peak}}}{\Gamma^2 m^2_{\rm e} c^4}$, where $E_{\gamma,{\rm peak}} = \max\,[E_{\gamma,{\rm c,s}}; E_{\gamma,{\rm m,s}}]$. The KN regime starts when $\kappa = 1$ (e.g. Fragile et al. 2004), and

$$E_{\gamma,{\rm K}} = \frac{\Gamma^2 m^2_{\rm e} c^4}{E_{\gamma,{\rm peak}}} = 2.5\ {\rm GeV} \frac{\Gamma^2_2}{E_{\gamma,{\rm peak,MeV}}}. \tag{22}$$

In the KN regime, the emissivity of electrons decreases by κ^2, and the photon energy spectral index simply follows the electron energy spectral index, that is, $-(p-2)$. The IC photon spectrum in equation (20) can be normalized as

$$\int_{E_{\gamma,{\rm m,i}}}^{E_{\gamma,{\rm max,i}}} E_{\gamma,{\rm i}} \frac{{\rm d}N_{\gamma,{\rm i}}(E_{\gamma,{\rm i}})}{{\rm d}E_{\gamma,{\rm i}}} {\rm d}E_{\gamma,{\rm i}} = E_{\rm iso} \frac{\eta_{\rm e}\epsilon_{\rm e} Y_{\rm e}}{1+Y_{\rm e}}, \tag{23}$$

where $E_{\gamma,{\rm max,i}} = \Gamma E'_{\rm e,max}$ is due to the KN effect.

4 PROTON SYNCHROTRON RADIATION

Relativistic protons lose energy by synchrotron radiation and photo-pion (π^0, π^+) production inside GRBs. They interact with the low-energy photons in the GRB environment and pions are produced. There is a threshold energy for this interaction (p–γ) to happen, $E_{\rm p} E_\gamma \geqslant 0.3\ {\rm GeV}^2 \Gamma^2$, where $E_{\rm p}$ and E_γ are proton, photon energy in the source rest frame, respectively. The π^0 s decay to a pair of high-energy photons, while the π^+ s decay to neutrinos and leptons. The threshold condition therefore suggests that the photon-pion related high-energy spectrum is typically more energetic than the electron IC spectrum. We assume that the proton spectrum in the internal shocks can be expressed as a power law in proton energy. We consider a proton spectral index similar to electrons for our present discussion. Since protons are poor emitters, we only consider the scenario of slow-cooling in the comoving proton spectrum:

$$\frac{{\rm d}N_{\rm p}(E'_{\rm p})}{{\rm d}E'_{\rm p}} \propto \begin{cases} E'^{\,-p}_{\rm p} & E'_{\rm p,m} < E'_{\rm p} < E'_{\rm p,c} \\ E'^{\,-p-1}_{\rm p} & E'_{\rm p,c} < E'_{\rm p} \end{cases}, \tag{24}$$

where $E'_{\rm p,m}$ is the minimum injection energy of the protons and $E'_{\rm p,c}$ is break energy in the spectrum due to proton cooling. The minimum injection energy $E'_{\rm p,m} = \bar{\gamma}'_{\rm p} m_{\rm p} c^2 g(p)$, where $g(p) = \frac{p-2}{p-1}$ for $p \gg 2$ and $g(p) \sim 1/6$ for $p = 2$. The cooling break energy can be derived by comparing the comoving and the cooling time-scales. The inverse of the cooling time-scale $t'_{\rm cool}$ of a proton is

$$\frac{1}{t'_{\rm cool}} = \frac{1}{t'_{\rm syn}} + \frac{1}{t'_\pi}. \tag{25}$$

The photo-pion cooling time-scale t'_π has been derived earlier in the context of estimation of neutrino fluxes from GRBs (Waxman & Bahcall 1997; Gupta & Zhang 2007). If f_π is the fraction of proton energy going to pion production in the Δ resonance of p–γ interactions, one

has $1/t'_\pi \sim f_\pi/t'_{\rm dyn}$ where the comoving time-scale is[2] $t'_{\rm dyn} = \Gamma\ t_{\rm v}$. The peak value of p–γ interaction cross-section at the Δ resonance is $\sigma_{p\gamma} = 5 \times 10^{-28}\,{\rm cm}^2$. This is much higher than the Thomson cross-section for protons $\sigma_{\rm p,T} = (\frac{m_{\rm e}}{m_{\rm p}})^2\sigma_{\rm e,T}$, where $\sigma_{\rm e,T} = 6.625 \times 10^{-25}\ {\rm cm}^2$. We therefore neglect the IC process of protons. Substituting for $t'_{\rm syn}$ and t'_π in equation (25), we get

$$\frac{1}{t'_{\rm cool}} = \frac{4}{3}\sigma_{\rm p,T}\beta_{\rm p}'^2\frac{E'_{\rm p}}{m_{\rm p}c^2}\frac{cU\epsilon_B}{m_{\rm p}c^2} + \frac{f_\pi}{\Gamma t_{\rm v}}, \tag{26}$$

where, $\beta'_{\rm p}$ is dimensionless speed of relativistic protons. We use the general expression for f_π from Gupta & Zhang (2007)

$$f_\pi(E_{\rm p}) = f_0\begin{cases}\frac{1.34^{\alpha_2-1}}{\alpha_2+1}\left(\frac{E_{\rm p}}{E_{\rm pb}}\right)^{\alpha_2-1} & E_{\rm p} < E_{\rm pb}\\ \frac{1.34^{\alpha_1-1}}{\alpha_1+1}\left(\frac{E_{\rm p}}{E_{\rm pb}}\right)^{\alpha_1-1} & E_{\rm p} > E_{\rm pb}\end{cases}, \tag{27}$$

where

$$f_0 = \frac{0.9L_{\rm iso,51}}{810\Gamma_2^4 t_{\rm v,-2}E_{\gamma,{\rm peak,MeV}}}\frac{1}{1/(\alpha_2-2)-1/(\alpha_1-2)}\frac{\eta_{\rm e}\epsilon_{\rm e}}{1+Y_{\rm e}}. \tag{28}$$

In our present discussion, $\alpha_2 = (p+2)/2$ and $\alpha_1 = (p+1)/2$. $E_{\gamma,{\rm peak,MeV}}$ is the peak energy in the electron synchrotron photon spectrum expressed in MeV, and $L_{\rm iso,51}$ is the GRB luminosity in unit of $10^{51}\,{\rm erg\,s^{-1}}$, which is the typical value for GRB luminosities. $E_{\rm pb} = 0.3\Gamma^2/E_{\gamma,{\rm peak,GeV}}$ GeV is the threshold proton energy for interaction with photons of energy $E_{\gamma,{\rm peak,GeV}}$. For typically observed values of GRB parameters one has $E_{\rm pb} \sim 1$ PeV. The break energy in the proton spectrum due to proton cooling can be calculated by comparing the comoving and cooling time-scales of protons as discussed in the case of electrons in Section 2. We assume $\beta'_{\rm p} \sim 1$ then for $E_{\rm p} < E_{\rm pb}$ the expression of cooling break energy in the comoving frame is

$$E'_{\rm p,c} = \frac{f_{\rm c}}{\Gamma t_{\rm v}}\left(\frac{4}{3}\sigma_{\rm p,T}\beta_{\rm p}'^2\frac{cU\epsilon_B}{m_{\rm p}^2c^4} + \frac{f_0}{E_{\rm pb}\Gamma t_{\rm v}}\frac{1.34^{\alpha_2-1}}{\alpha_2+1}\right)^{-1} = \frac{10^8\ {\rm GeV}\,f_{c,2}}{\Gamma_2 t_{\rm v,-2}}\left(0.16\frac{L_{\rm iso,51}\epsilon_B}{\Gamma_2{}^6 t_{\rm v,-2}^2} + \frac{f_0}{E_{\rm pb}({\rm PeV})\Gamma_2 t_{\rm v,-2}}\frac{1.34^{\alpha_2-1}}{\alpha_2+1}\right)^{-1}, \tag{29}$$

where $f_{\rm c} = \frac{t'_{\rm dyn}}{t'_{\rm cool}}$. The synchrotron photon spectrum from relativistic protons is

$$E_{\gamma,{\rm ps}}^2\frac{{\rm d}N_{\gamma,{\rm ps}}(E_{\gamma,{\rm ps}})}{{\rm d}E_{\gamma,{\rm ps}}} \propto \begin{cases}E_{\gamma,{\rm ps}}^{-(p-3)/2} & E_{\gamma,m,{\rm ps}} < E_{\gamma,{\rm ps}} \leqslant E_{\gamma,{\rm c,ps}}\\ E_{\gamma,{\rm c,ps}}^{1/2}E_{\gamma,{\rm ps}}^{-(p-2)/2} & E_{\gamma,{\rm c,ps}} < E_{\gamma,{\rm ps}}\end{cases} \tag{30}$$

The minimum injection energy in the photon spectrum from proton synchrotron radiation is related to that from electron synchrotron radiation as (Zhang & Mészáros 2001):

$$\frac{E_{\gamma,m,{\rm ps}}}{E_{\gamma,{\rm m,s}}} = \left(\frac{E'_{\rm p,m}}{E'_{\rm e,m}}\right)^2\left(\frac{m_{\rm e}}{m_{\rm p}}\right)^3. \tag{31}$$

The cooling break energy in the photon spectrum from proton synchrotron radiation is the characteristic synchrotron photon energy for proton energy $E'_{\rm p,c}$. To normalize the proton synchrotron spectrum, it is important to find out the relative importance between proton synchrotron radiation and p–γ interactions. Similar to the treatment of electrons, one can define

$$Y_{\rm p} = \frac{L_{{\rm p},p\gamma}}{L_{\rm p,syn}} = \frac{\sigma_{p\gamma}}{\sigma_{\rm p,T}}\frac{U_{\rm e,syn}}{U_B} = \frac{\sigma_{p\gamma}}{\sigma_{\rm p,T}}Y_{\rm e}, \tag{32}$$

where $L_{{\rm p},p\gamma}$ and $L_{\rm p,syn}$ are the luminosities of radiations emitted in p–γ interactions and synchrotron emission of protons, respectively. Note that protons interact with the synchrotron emission of the electrons, so that $Y_{\rm e}$ enters the problem. Equation (32) suggests that $Y_{\rm p}$ is usually much greater than unity since $\sigma_{p\gamma} \gg \sigma_{\rm p,T}$. As a result, most of the proton energy is lost through p–γ interaction rather than proton synchrotron radiation.

The proton synchrotron photon spectrum can be normalized as

$$\int_{E_{\gamma,m,{\rm ps}}}^{E_{\gamma,{\rm max,ps}}} E_{\gamma,{\rm ps}}\frac{{\rm d}N_{\gamma,{\rm ps}}(E_{\gamma,{\rm ps}})}{{\rm d}E_{\gamma,{\rm ps}}}{\rm d}E_{\gamma,{\rm ps}} = E_{\rm iso}\frac{\epsilon_{\rm p}\eta_{\rm p}}{1+Y_{\rm p}}, \tag{33}$$

where $\eta_{\rm p} = (E'_{\rm p,c}/E'_{\rm p,m})^{2-\alpha}$. The maximum proton synchrotron photon energy is derived by $E_{\gamma,{\rm max,ps}} = \Gamma\frac{3h}{4\pi}(\frac{E'_{\rm p,max}}{m_{\rm p}c^2})^2\frac{eB'c}{m_{\rm p}c^2}$, where $E'_{\rm p,max}$ is again defined by comparing the comoving acceleration time with the shorter of the comoving dynamical and cooling times scales

$$E'_{\rm p,max} = \min\left[50\left(\frac{B'_6\Gamma_2^6 t_{\rm v,-2}^2}{L_{\rm iso,51}\epsilon_B(1+Y_{\rm p})}\right)^{1/2}, 1.4\times10^6\Gamma_2 t_{\rm v,-2}B'_6\right]\ {\rm TeV}. \tag{34}$$

or

$$E'_{\rm p,max} = \min\left[191\left(\left(\frac{\xi_1}{\epsilon_{B,-1}L_{\rm iso,51}}\right)^{1/2}\frac{\Gamma_2^3 t_{\rm v,-2}}{1+Y_{\rm p}}\right)^{1/2}, \frac{208}{\Gamma_2^2}\times10^4(\xi_1\epsilon_{B,-1}L_{\rm iso,51})^{1/2}\right]\ {\rm TeV}. \tag{35}$$

[2] In this definition, on average protons loose ∼20 per cent energy in the time-scale of t'_π. Although it is not strictly the e-folding time-scale usually used to define cooling, for order-of-magnitude estimates this is good enough.

5 π^0 DECAY

The relativistic protons interact with the low-energy photons and photo-pions (π^0, π^+) are produced as a result. The probabilities of π^0 and π^+ production are 1/3 and 2/3, respectively. Pions subsequently decay, that is, $\pi^0 \rightarrow \gamma\gamma$ and $\pi^+ \rightarrow \mu^+\nu_\mu \rightarrow \nu_\mu \bar{\nu}_\mu \nu_e e^+$. As the cross-section for the $\gamma\gamma$ interactions is much higher than the peak value of p–γ interaction cross-section, above the threshold energy of pair production $\gamma\gamma$ interactions are expected to dominate over p–γ interactions. If the photon energy is $2m_e c^2 \sim 1$ MeV in the comoving frame, then in the source rest frame it is of the order of a few hundred MeV as the Lorentz factors are typically of the order of few hundred for canonical GRBs. For example, for $\Gamma = 400$ the photons of energy 400 MeV can produce photo-pions by interaction with protons of minimum energy $E_p \sim 120$ TeV. The π^0 typically carries 20 per cent of the proton's energy and the photons produced in π^0 decay share its energy equally. Hence, the minimum energy of the photons produced from π^0 decay is expected to be $\sim$10 per cent $E_p \sim 12$ TeV. The photon spectrum produced from π^0 decay has been derived below using the proton spectrum defined in equation (24) and assuming the fraction $f_\pi/3$ of protons' energy goes to π^0 s:

$$E^2_{\gamma,\pi^0}\frac{\mathrm{d}N_{\gamma,\pi^0}(E_{\gamma,\pi^0})}{\mathrm{d}E_{\gamma,\pi^0}} \propto \frac{1}{3}\frac{f_\pi(E_{\gamma,\pi^0})}{2}\begin{cases} E^{2-p}_{\gamma,\pi^0} & E_{\gamma,\pi^0} \leqslant E_{\gamma,\pi^0,\mathrm{c}} \\ E^{1-p}_{\gamma,\pi^0} & E_{\gamma,\pi^0} > E_{\gamma,\pi^0,\mathrm{c}} \end{cases}, \tag{36}$$

where, $E_{\gamma,\pi^0,\mathrm{c}} = 0.1E_{\mathrm{p,c}}$. For the expression for f_π, see equation (27), which contains a break energy. The break energy in the photon spectrum contained within f_π is $E_{\gamma,\pi^0,\mathrm{b}} = 0.03\Gamma^2/\epsilon_{\mathrm{br,GeV}}$ GeV assuming 10 per cent of the proton's energy goes to the photon produced via π^0 decay. ϵ_{br} is the break energy in the low-energy photon spectrum (in the scenario of slowly cooling electrons it is the cooling break energy in the photon spectrum and for fast cooling electrons it is the photon energy corresponding to the minimum injection energy of electrons). The photon flux can be normalized in the following way:

$$\int_{E_{\gamma,\pi^0,\mathrm{min}}}^{E_{\gamma,\pi^0,\mathrm{max}}} E_{\gamma,\pi^0}\frac{\mathrm{d}N_{\gamma,\pi^0}(E_{\gamma,\pi^0})}{\mathrm{d}E_{\gamma,\pi^0}}\mathrm{d}E_{\gamma,\pi^0} = \frac{E_{\mathrm{iso}}}{3}\frac{\epsilon_{\mathrm{p}}\eta_{\mathrm{p}}Y_{\mathrm{p}}}{1+Y_{\mathrm{p}}}, \tag{37}$$

where $E_{\gamma,\pi^0,\mathrm{min}=30\Gamma}$ GeV and $E_{\gamma,\pi^0,\mathrm{max}} = 0.1E_{\mathrm{p,max}}$. Although high-energy photons ($\sim$ TeV) are absorbed by lower energy photons and e^+e^- pairs are produced, at extreme energies the pair production cross-section decreases with increasing energy (Razzaque et al. 2004). Hence, ultrahigh-energy photons can escape from the internal shocks for suitable parameters depending on the values of their various parameters and the low-energy photon spectra.

6 SYNCHROTRON RADIATION OF POSITRONS PRODUCED IN π^+ DECAY

The shock-accelerated protons may interact with the low-energy photons to produce π^+ s along with π^0 s as discussed in the previous section. The π^+ s subsequently decay to muons and neutrinos. The energetic muons decay to positrons and neutrinos ($p\gamma \rightarrow \pi^+ \rightarrow \mu^+\nu_\mu \rightarrow e^+\nu_\mu\bar{\nu}_\mu\nu_e$). The charged pions, muons and the positrons are expected to lose energy through synchrotron radiation and IC inside the shock region. As the Thomson cross-section for positrons is much larger than pions or muons, they are expected to emit much more radiation compared to the heavier charged particles. On the other hand, since these positrons are very energetic, most IC processes happen in the KN regime. We therefore neglect the contribution of the positron IC processes. The positron synchrotron spectrum produced in p–γ interactions can be derived in the following way. The fraction of the protons' energy tranferred to pions is denoted by f_π (equation [27]). If we assume that the final state leptons share the pion's energy equally then one fourth of the pion's energy goes to the positron. The energy of the positron spectrum $\frac{\mathrm{d}N(E_{e^+})}{\mathrm{d}E_{\mathrm{e}^+}}$ at the energy E_{e^+} can be expressed using the proton spectrum defined in equation (24):

$$E^2_{e^+}\frac{\mathrm{d}N(E_{e^+})}{\mathrm{d}E_{e^+}} \propto \frac{2}{3}\frac{f_\pi(E_{e^+})}{4}\begin{cases} E^{2-p}_{e^+} & E_{e^+} \leqslant E_{e^+,c} \\ E^{1-p}_{e^+} & E_{e^+} > E_{e^+,c} \end{cases}, \tag{38}$$

where, $E_{e^+,c}$ is the cooling break energy in the positron specrum and

$$f_\pi(E_{\mathrm{e}^+}) = f_0\begin{cases} \frac{1.34^{\alpha_2-1}}{\alpha_2+1}\left(\frac{E_{\mathrm{e}^+}}{E_{e^+b}}\right)^{\alpha_2-1} & E_{\mathrm{e}^+} < E_{\mathrm{e}^+\mathrm{b}} \\ \frac{1.34^{\alpha_1-1}}{\alpha_1+1}\left(\frac{E_{\mathrm{e}^+}}{E_{e^+b}}\right)^{\alpha_1-1} & E_{e^+} > E_{e^+b} \end{cases}, \tag{39}$$

where f_0 has been defined in equation (28), $E_{\mathrm{e}^+\mathrm{b}} = 0.05E_{\mathrm{pb}}$, $E_{\mathrm{pb}} = 0.3\ \mathrm{GeV}\Gamma^2/\epsilon_{\mathrm{br,GeV}}$, and $\epsilon_{\mathrm{br,GeV}}$ is the break energy in the photon spectrum as defined earlier. The positron spectrum in equation (38) can be normalized using the total energy carried by the positrons,

$$\int_{E_{e^+,\mathrm{min}}}^{E_{\mathrm{e}^+,\mathrm{max}}} E_{\mathrm{e}^+}\frac{\mathrm{d}N(E_{\mathrm{e}^+})(E_{\mathrm{e}^+})}{\mathrm{d}E_{\mathrm{e}^+}}\mathrm{d}E_{\mathrm{e}^+} = \frac{1}{6}\frac{\epsilon_{\mathrm{p}}\eta_{\mathrm{p}}Y_{\mathrm{p}}E_{\mathrm{iso}}}{1+Y_{\mathrm{p}}}. \tag{40}$$

The maximum and minimum positron energies are $E_{\mathrm{e}^+,\mathrm{max}} = 0.05E_{\mathrm{p,max}}$ and $E_{e^+,\mathrm{min}} = 15\Gamma$ GeV (which is $\sim$6 TeV for $\Gamma = 400$). The synchrotron photon spectrum from the positrons can be subsequently derived using the same treatment for primary electrons as discussed in Section 2. The IC emission is in the KN regime and therefore not important. Also, photons having energies above a few hundred GeV are annihilated by lower energy photons as discussed in the following section. The relativistic muons produced in π^+ decay lose energy by synchrotron radiation. We compare the decay and synchrotron energy loss time-scales of the high-energy muons. The maximum energies of positrons can be calculated in this way. If the muons decay before losing energy significantly high-energy positrons are produced carrying

approximately 5 per cent of the initial proton's energy. On the other hand, if the muons lose energy before they decay lower energy positrons are produced. These positrons radiate energy and produce lower energy photons. The muons initially carry approximately 10 per cent of the relativistic protons' energy hence, we expect the low-energy photon flux produced by cooling of positrons is lower than that produced by relativistic electrons if ϵ_e and ϵ_p are comparable.

7 INTERNAL PAIR-PRODUCTION OPTICAL DEPTHS OF HIGH-ENERGY PHOTONS

Inside GRBs high-energy photons interact with low-energy photons to produce electron-positron pairs (e.g. Baring & Harding 1997; Lithwick & Sari 2001). The optical depth depends on the values of various parameters of the GRB fireball. We follow the approach discussed in Bhattacharjee & Gupta (2003) to derive internal optical depths of GRBs in detail. For two photons (a high-energy photon γ_h and a low-energy photon γ_l), the pair production cross-section depends on the energies of the photons and the angle between their directions of propagation. The cross-section is (Berestetskii, Lifshitz & Pitaevskii 1982):

$$\sigma_{\gamma_h\gamma_l}(E'_{\gamma_h}, E'_{\gamma_l}, \theta) = \frac{3}{16}\sigma_T(1-\beta'^2)\left[(3-\beta'^4)\ln\frac{1+\beta'}{1+\beta'} - 2\beta'(2-\beta'^2)\right], \tag{41}$$

where σ_T is the Thomson cross-section, and $\beta' = [1-(E'_{\gamma_l,th}/E'_{\gamma_l})]^{1/2}$ is the centre of mass dimensionless speed of the pair produced. The threshold energy of pair production with a high-energy photon of energy E'_{γ_h} is

$$E'_{\gamma_l,th} = \frac{2(m_e c^2)^2}{E'_{\gamma_h}(1-cos\theta)}. \tag{42}$$

For the photons with energy higher than the threshold energy, the pair production cross-section decreases with increasing photon energy (Jauch & Rohrlich 1955; Razzaque et al. 2004). In this work, we calculate internal optical depths in different energy regimes using the cross-sections with different energy dependencies. The mean free path for γ_h γ_l interactions $l_{\gamma_h\gamma_l}$ can be calculated using the low-energy photon spectrum:

$$l^{-1}_{\gamma_h\gamma_l\theta}(E'_{\gamma_h}, \theta) = \int_{E'_{\gamma_l,th}}^{\infty} dE'_{\gamma_l}\frac{dn_{\gamma_l}(E'_{\gamma_l})}{dE'_{\gamma_l}}\sigma_{\gamma_h\gamma_l}\left(E'_{\gamma_h}, E'_{\gamma_l}, \theta\right), \tag{43}$$

and

$$l^{-1}_{\gamma_h\gamma_l}(E'_{\gamma_h}) = \frac{1}{2}\int_{-1}^{+1} d(\cos\theta)(1-\cos\theta)l^{-1}_{\gamma_h\gamma_l\theta}(E'_{\gamma_h}, \theta), \tag{44}$$

where $\frac{dn_{\gamma_l}(E'_{\gamma_l})}{dE'_{\gamma_l}}$ is the specific number density of low-energy photons inside the GRB. The low-energy photon spectrum is observationally known, as revealed by gamma-ray detectors such as BATSE and *Swift*. Theoretically, it corresponds to the electron synchrotron component as discussed in Section 2, which is a broken power-law spectrum separated by the synchrotron self-absorption break, the minimum injection break and the cooling break. The low-energy photon flux is related to the observed luminosity through

$$\int_{E'_{\gamma_l,ssa}}^{E'_{\gamma_l,max}} E_{\gamma_l}{}'\frac{dn_{\gamma_l}(E'_{\gamma_l})}{dE'_{\gamma_l}}dE_{\gamma_l}{}' = U_\gamma = \frac{L_{\gamma,iso}}{4\pi c r_{is}{}^2\Gamma^2}, \tag{45}$$

where $L_{\gamma,iso}$ is the isotropic gamma-ray luminosity. We have taken it to be equal to the luminosity of the synchrotron photons emitted by electrons: $L_{\gamma,iso} = L_{e,syn} = \frac{\epsilon_e\eta_e L_{iso}}{1+Y_e}$. In equation (44) we have three variables: angle θ and photon energies E'_{γ_l} and E'_{γ_h}. To simplify the integration in equation (44), we transform the integral with a new variable following Gould & Schreder (1967):

$$s = \frac{E'_{\gamma_l}E'_{\gamma_h}(1-\cos\theta)}{2(m_e c^2)^2} = \frac{E'_{\gamma_l}}{E'_{\gamma_l,th}} = s_0\Theta \tag{46}$$

with $s_0 = \frac{E'_{\gamma_l}E'_{\gamma_h}}{(m_e c^2)^2}$, and $\Theta = \frac{1}{2}(1-\cos\theta)$. As $\beta' = (1-1/s)^{1/2}$, the pair production cross-section can be expressed as a function of the new variable s. It is then possible to write equation (44) as

$$l^{-1}_{\gamma_h\gamma_l}(E'_{\gamma_h}) = \frac{3}{8}\sigma_T\left(\frac{m_e^2c^4}{E'_{\gamma_h}}\right)^2\int_{\frac{m_e^2c^4}{E'_{\gamma_h}}}^{\infty}\left[E'_{\gamma_l}{}^{-2}\frac{dn_{\gamma_l}(E'_{\gamma_l})}{dE'_{\gamma_l}}dE'_{\gamma l}\right]Q\left[s_0\left(E'_{\gamma_l}\right)\right], \tag{47}$$

where

$$Q[s_0(E'_{\gamma_l})] = \int_1^{s_0(E'_{\gamma_l})} s\sigma(s)\,ds, \tag{48}$$

and $\sigma(s) = \frac{16}{3}\frac{\sigma_{\gamma_h\gamma_l}}{\sigma_T}$. For moderate values of s we use $\sigma(s) \simeq 1$ and for $s \gg 1$ it can be approximated as $\sigma(s) \simeq \ln(s)/s$. The expressions for $Q[s_0(E'_{\gamma_l})]$ are $(s_0^2-1)/2$ and $s_0(\ln s_0 - 1)$, respectively, in the two cases. Substituting for $Q[s_0(E'_{\gamma_l})]$ in equation (47) we derive the final expression for $l^{-1}_{\gamma_h\gamma_l}(E'_{\gamma_h})$. The internal optical depth $\tau_{int}(E'_{\gamma_h})$ is the ratio of comoving time-scale and the mean time between two pair production interactions:

$$\tau_{int}(E'_{\gamma_h}) = \frac{r_{is}}{\Gamma c}cl^{-1}_{\gamma_h\gamma_l}(E'_{\gamma_h}). \tag{49}$$

The final photon energy spectrum to be observed on Earth from nearby GRBs (neglecting further attenuations with the infrared background and cosmic microwave background) can be obtained by correcting the original flux for the internal optical depth and the redshift z of the source:

$$E_{\gamma,\rm ob}^2 \frac{{\rm d}N_{\gamma,\rm ob}(E_{\gamma,\rm ob})}{{\rm d}E_{\gamma,\rm ob}} = \frac{1}{4\pi d_z^2(1+z)} E_\gamma^2 \frac{{\rm d}N_\gamma(E_\gamma)}{{\rm d}E_\gamma} \exp[-\tau_{\rm int}(E_\gamma)], \tag{50}$$

where

$$d_z = \frac{c}{H_0} \int_0^z \frac{dz'}{\sqrt{\Omega_\Lambda + \Omega_{\rm m}(1+z')^3}} \tag{51}$$

is the comoving distance of the source, $H_0 = 71\,{\rm km\,s^{-1}\,Mpc^{-1}}$ is the Hubble constant, and $\Omega_\Lambda = 0.73$ and $\Omega_{\rm m} = 0.27$ are adopted in our calculations.

8 PHOTON SPECTRUM FROM SECONDARY ELECTRONS AND POSITRONS

The secondary pairs carry a significant fraction of energy in the primary spectrum, and this energy is re-radiated and converted to photons. A more realistic treatment should consider a photon-pair cascade process, which requires numerical calculations (Pe'er & Waxman 2004; Pe'er et al. 2006). Here instead we estimate the emission from the secondary pairs. We first calculate the photon energy spectra generated by different physical processes as discussed earlier. The photon spectra are then corrected for internal optical depths and subsequently the total energies carried by these photons are calculated by integrating the corrected photon energy spectra over photon energies. If we subtract the total energies carried by these high-energy photons from their intial energies before including the effects of internal optical depths, we get the energies of the secondary e^- and e^+ produced in $\gamma\gamma$ interactions. These pairs are expected to have spectral indices similar to the high-energy photons. With the knowledge of their spectral indices and the total energies carried by them the synchrotron photon spectra radiated by these secondary leptons are calculated. For the parameters adopted in this paper, it turns out that the emission contribution from the secondaries is below the emission level of the primaries, and hence, does not significantly modify the observed the spectrum. We therefore do not include this component in Figs 1–5, but caution that such a feedback process could be potentially important for the parameter regimes with high opacity. We refer to Pe'er & Waxman (2004) and Pe'er et al. (2006) for more detailed treatments of such cases.

9 SYNTHESIZED SPECTRA AND DETECTABILITY

Using the procedure delineated above, we have calculated the broad-band emission spectrum from internal shocks for a wide range of parameter regimes. In particular we focus on the various high-energy emission components discussed above and their relative significance. Our results are presented in Figs 1–5. In each set of calculations we have presented the internal optical depth after the final photon energy spectrum. For particles accelerated by ultrarelativistic shocks the spectral index is expected to be about 2.26 Lemoine & Pelletier (2003). Afterglow modelling suggests a larger scatter of p values for relativistic shocks, but $p = 2.3$ is close the mean value of the data (Panaitescu & Kumar 2000). In all our calculations, the spectral indices of relativistic electrons and protons are both assumed as $p = 2.3$.

Figs 1–4 are the calculations for a typical long GRB with duration $T_{90} = 20$ s at redshift $z = 1$ (10 s in the source rest frame). Since we do not know the physical condition of the internal shocks from the first principles, we vary the parameter regime in a wide range. In each set of calculations, we design the parameters to make the electron synchrotron emission peaking at the sub-MeV range ($\sim$0.36, 0.13, 0.6 and 0.25 MeV for Figs 1, 2, 3 and 4, respectively), as suggested by the data. The global energetics of the GRB is also adjusted so that the gamma-ray luminosity in the sub-MeV range is about $10^{51}\,{\rm erg\,s^{-1}}$ as suggested by the observations. The variability time-scale for these calculations is taken as $t_{\rm v} = 0.01$ s. The bulk Lorentz factor is adopted as $\Gamma = 400$ in Figs 1–3, as suggested by the recent early optical afterglow observations (Molinari et al. 2007). In order to check how Γ affects the spectra, we also calculate the case of $\Gamma = 1000$ for the parameter set of Fig. 1, which is presented in Fig. 4. In all the figures, the different components of the photon energy spectrum from a GRB for both electrons (e) and protons (p) are displayed with different line styles/colours. The observed energy fluxes $E_{\gamma,\rm ob}^2 \frac{{\rm d}N_{\gamma,\rm ob}(E_{\gamma,\rm ob})}{E_{\gamma,\rm ob}}$ in unit of erg cm^{-2} s^{-1} are plotted against the observed photon energy $E_{\gamma,\rm ob}$(eV). The green long dashed curves represent the synchrotron emission from the relativistic electrons. The short dashed curves (blue) represent the IC spectrum from energetic electrons; the dash–dotted curves (light blue) represents the synchrotron emission of the relativistic protons; the triple short dashed curves (orange) represent for the synchrotron emission of the relativistic positrons produced in π^+ decays; the ultrahigh-energy emission component from π^0 decays is shown by the double short dashed curves (black) in the extremely high-energy regime. The thin black solid lines represent the synthesized spectra of various components without including the effect of pair production attenuation. Depending on parameters, the pair opacity becomes important in the GeV–TeV range. The thick black solid lines represent the final photon spectrum after including the internal optical depths. In order to check whether the predicted high-energy components are detectable by GLAST, we also plot an indicative GLAST sensitivity threshold in the 100 MeV–100 GeV energy range. The GLAST sensitivity estimate is based on the criterion of detecting at least a few photons in the band based on the average effective area and photon incoming zenith angle of LAT. Background is negligible for GRB detections. This gives a rough fluence threshold of $\sim 2 \times 10^{-7}\,{\rm erg\,cm^{-2}}$ (B. Dingus, 2007, private communication). The flux thresholds adopted in all the figures are therefore derived from the observed durations. For $T_{90} = 20$ s, this gives a flux threshold of $\sim 10^{-8}\,{\rm erg\,cm^{-2}\,s^{-1}}$. The sensitivity of VERITAS to photon above energy 200 GeV has also been shown in our figures with pink dotted line. It is $2 \times 10^{-8}\,{\rm erg\,cm^{-2}\,s^{-1}}$ (D. Horan, 2007, private communication).

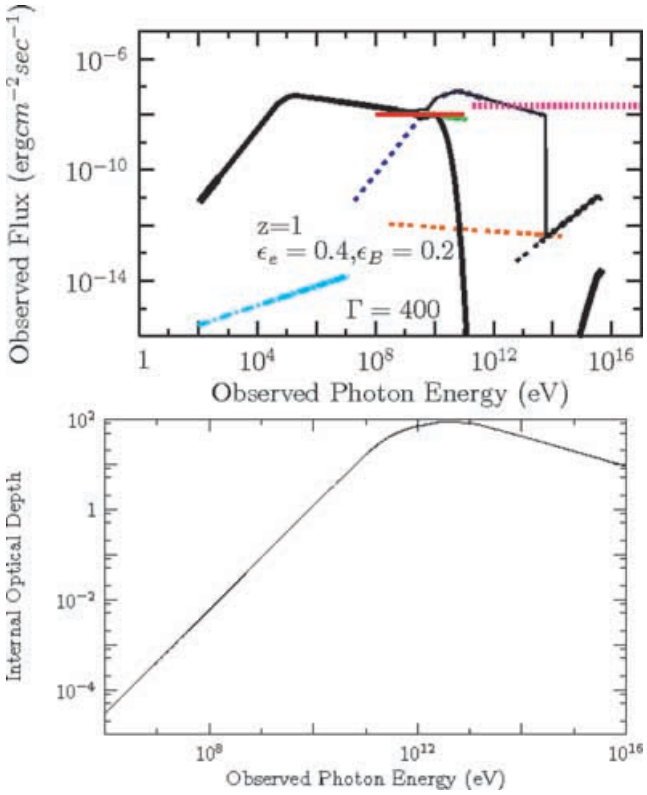

Figure 1. A leptonic-component-dominated slow cooling spectrum. (a): the different components of the photon energy spectrum from the internal shocks for the following parameters in the slow-cooling regime: $E_{\rm iso} = 10^{53}$ erg, $L_{\rm iso} = 10^{52}$ erg s^{-1}, $t_{\rm v} = 0.01$ s and $f_{\rm c} = 2500$. The thick solid black curve represents the final spectrum after including the effect of internal optical depths. The thin solid black curve represents the synthesized spectrum before including the effect of internal optical depths. The long dashed (green) curve is the electron synchrotron component; the short dashed (blue) curve is the electron IC component; the double short dashed (black) curve on the right side is for π^0 decay component; the triple short dashed (orange) line represents the synchrotron radiation produced by positrons generated in π^+ decays; the dash–dotted (light blue) line represents the proton synchrotron component. The tiny red horizontal line between 10^8 and 10^{11} eV represents GLAST's threshold. The pink dotted horizontal line above 2×10^{11} eV represents the sensitivity of VERITAS experiment. (b) Internal optical depths plotted against energy for the parameters adopted in (a).

Fig. 1 is a standard 'slow-cooling' leptonic-dominant case. The shock equipartition parameters are $\epsilon_{\rm e} = 0.4$ and $\epsilon_B = 0.2$. The isotropic shock luminosity is $L_{\rm iso} = 10^{52}$ erg s^{-1}. The slow cooling factor $f_{\rm c} = 2500$ is adopted, which suggests that the post-shock magnetic field decays on a length-scale shorter than the comoving scale (Pe'er & Zhang 2006). The thick black line shown on the right side around 10^{15} eV is the π^0 component after including the effect of absorption due to pair production, indicating the reduction of pair opacity at high energies (Fig. 1b, see also Razzaque et al. 2004). In this figure, the break energies in the photon energy spectrum appear of the order of $E_{\rm ssa} < E_{\gamma,{\rm m}} < E_{\gamma,{\rm c}}$ in the electron synchrotron and IC spectral components. The spectral index of the photon energy spectrum is 4/3 between $E_{\rm ssa}$ and $E_{\gamma,{\rm m}}$, $-(p - 3)/2$ between $E_{\gamma,{\rm m}}$ and $E_{\gamma,{\rm c}}$, and $-(p-2)/2$ above $E_{\gamma,{\rm c}}$. Since $\epsilon_{\rm e}$ is large, the leptonic components are many orders of magnitude stronger than the hadronic components. The value of $Y_{\rm p}$ is much larger than 1, so that the proton synchrotron component is below the components due to π^0 decay and positron synchrotron radiation.

We vary the values of the equipartition parameters ($\epsilon_{\rm e}$, ϵ_B, $\epsilon_{\rm p}$) and study the variations in the photon energy fluxes generated by various processes. The emission level of the electron IC spectral component decreases with decreasing $\epsilon_{\rm e}$ (fixing ϵ_B) since $Y_{\rm e}$ is decreasing. Moreover, as we decrease $\epsilon_{\rm e}$ the minimum injection energy of electrons $E_{\gamma,{\rm m}}$ also decreases. In the slow cooling regimes, it is $E_{\gamma,{\rm c}}$ that defines the peak energy in the electron synchrotron spectrum, which could be adjusted to the sub-MeV range by adopting a suitable $f_{\rm c}$ value. The change in $E_{\gamma,{\rm m}}$ therefore mainly affects the calculated internal optical depth.

By lowering $\epsilon_{\rm e}$, we check the parameter regime where the hadronic component becomes comparable. Since eletrons are much more efficient emitters than protons, the parameter regime for the hadronic component to be comparable to the leptonic component in the high-energy regime is $\epsilon_{\rm e}/\epsilon_{\rm p} \sim m_{\rm e}/m_{\rm p} < 10^{-3}$.[3] A similar conclusion has been drawn for the external shocks (Zhang & Mészáros 2001). In Fig. 2, with $\epsilon_{\rm e} = 10^{-3}$, $\epsilon_B = 0.05$ and $\epsilon_{\rm p} = 0.849$. In order to adjust $E_{\gamma,{\rm c}}$ to the sub-MeV range, $f_{\rm c} = 50000$ is needed. In order to match the observed

[3] Proton energy loss and their contribution to high-energy photon emission in the early afterglow phase has been studied earlier by Pe'er & Waxman (2005). Our results for the prompt emission phase are generally consistent with them. In order for the proton synchrotron component to be significant, even smaller $\epsilon_{\rm e}$ (than 10^{-3}) is demanded. Considering that photon-pion emission is more efficient than proton synchrotron emission, the condition $\epsilon_{\rm e}/\epsilon_{\rm p} \sim m_{\rm e}/m_{\rm p} < 10^{-3}$ can allow the hadronic components to be comparable to (but not dominant over) the leptonic components.

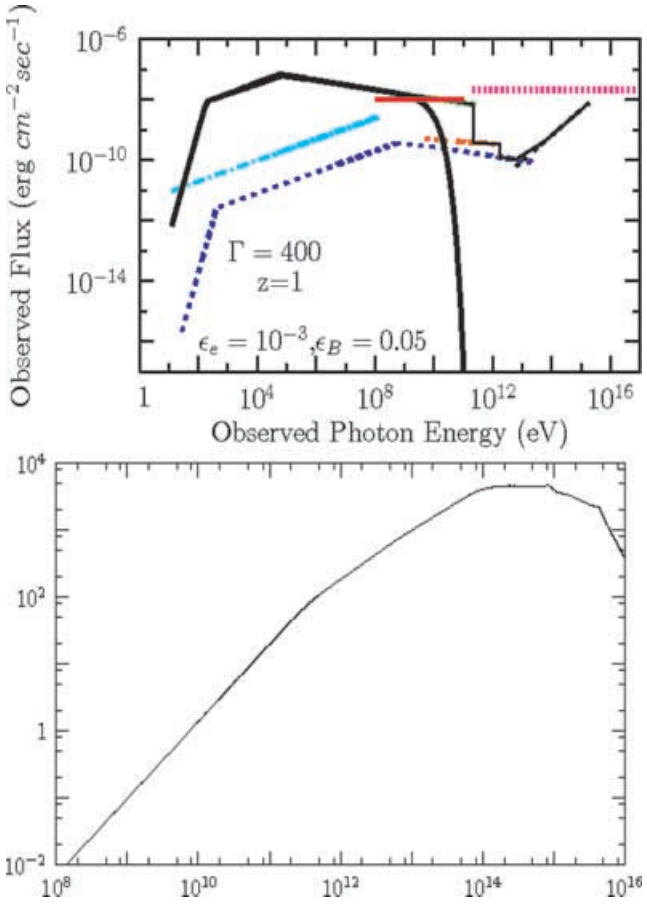

Figure 2. A slow-cooling spectrum with significant hadronic contribution. (a): The spectra of various components. Parameters: $\epsilon_e = 10^{-3}$, $\epsilon_B = 0.05$, $\epsilon_p = 0.849$, $t_v = 0.01$ s, $f_c = 50000$, $E_{iso} = 10^{56}$ erg and $L_{iso} = 10^{55}$ erg s^{-1}. The same line styles have been used as in Fig. 1. (b): The corresponding internal optical depths.

MeV emission flux by electron synchrotron, a large energy budget is needed due to a small ϵ_e: $E_{iso} = 10^{56}$ erg and $L_{iso} = 10^{55}$ erg s^{-1}. Such a large energy budget has been suggested before (Totani 1998), but afterglow observations and modelling in the pre-*Swift* era have generally disfavored such a possibility (Panaitescu & Kumar 2002). In the *Swift* era, however, a large afterglow kinetic energy for some GRBs is not ruled out. For example, the bright afterglow of GRB 061007 demands a huge kinetic energy if the afterglow is produced by isotropic external shocks (Mundell et al. 2007; Schady et al. 2007). Modelling some X-ray afterglows below the cooling frequency requires a low ϵ_B and/or a large afterglow kinetic energy at least for some GRBs (Zhang et al. 2007). We therefore still consider such a possibility. In Fig. 2, the break energy in the photon energy spectrum due to the minimum injection energy of electrons is below the synchrotron self-absorption energy. The break energies appear of the order of $E_{\gamma,m} < E_{ssa} < E_{\gamma,c}$ in the synchrotron and IC electron spectra. The spectral index of the photon energy flux is 7/2 between $E_{\gamma,m}$ and E_{ssa}, $-(p-3)/2$ between E_{ssa} and $E_{\gamma,c}$, and $-(p-2)/2$ above $E_{\gamma,c}$. We can see that in the TeV energy regime beyond the maximum electron synchrotron energy, the positron synchrotron emission from π^+ decay becomes dominant. Moreover, when ϵ_e is small, Y_e is small, hence Y_p becomes small. In this case the proton synchrotron component becomes comparable to the spectral components due to synchrotron radiation of the secondary positrons and π^0 decays. The internal optical depth is plotted in Fig. 2(b), which peaks at a higher energy than that in Fig. 1(b).

If the post-shock magnetic field does not decay within a short distance ($f_c = 1$), internal shocks are in the standard fast-cooling regime. We calculate such a case in Fig. 3. The shock parameters are $\epsilon_e = 0.6$, $\epsilon_B = 0.2$, $L_{iso} = 10^{52}$ erg s^{-1}, $E_{iso} = 10^{53}$ erg. In this case, the break energies appear as of the order of $E_C < E_{ssa} < E_m$. The photon energy spectral indices are 13/8, 1/2 and $-(p-2)/2$, respectively, in the three energy regimes.

The pair opacity depends on the bulk Lorentz factor. When Γ is large enough, the ultrahigh-energy photons would have lower internal optical depth and may escape from the internal shocks (Razzaque et al. 2004). To test this, in Fig. 4, we re-calculate with the parameter set for Fig. 1, but increase Γ to 1000. The slow-cooling parameter f_c is adjusted to 50 to maintain the sub-MeV energy peak. The results indeed suggest that the attenuation of the high-energy photons is weaker.

The observational breakthough in 2005 suggests that at least some short GRBs are low-fluence, nearby events that have a distinct progenitor than long GRBs (Barthelmy et al. 2005; Berger et al. 2005; Fox et al. 2005; Gehrels et al. 2005; Villasenor et al. 2005; Bloom et al. 2006). To check the prospect of detecting short GRB prompt emission with high-energy detectors such as GLAST, we perform a calculation

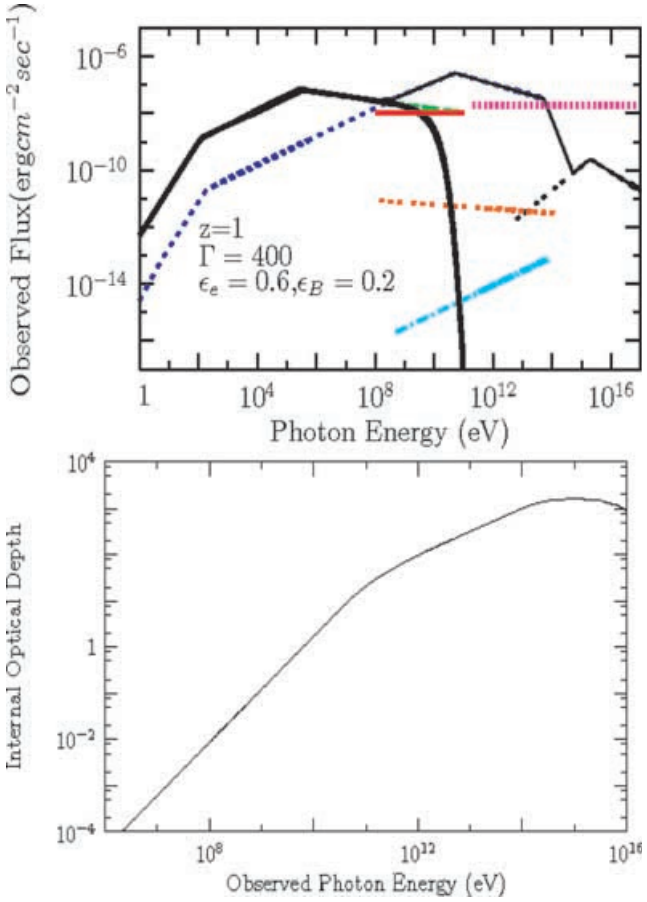

Figure 3. A leptonic-component-dominated fast-cooling spectrum. (a): The spectra of various components. Parameters: $\epsilon_e = 0.6$, $\epsilon_B = 0.2$, $\epsilon_p = 0.2$, $t_v = 0.01$ s, $f_c = 1$, $E_{iso} = 10^{53}$ erg and $L_{iso} = 10^{52}$ erg s^{-1}. The same line styles have been used as in Fig. 1. (b): The corresponding internal optical depths.

for the parameters of a short GRB in Fig. 5. Due to their short durations, short GRB detections are favorable for high luminosity and relatively 'long durations'. We therefore take an optimistic set of parameters with $L_{iso} = 10^{51}$ erg s^{-1}, $T_{90} = 1$ s, and $z = 0.1$. Other parameters include: $\Gamma = 800$, $t_v = 1$ ms, $\epsilon_e = 0.4$, $\epsilon_B = 0.2$, $\epsilon_p = 0.4$, $f_c = 50$. The photon flux from synchrotron radiation of electrons peaks at 0.1 MeV. Fig. 5(a) suggests that the high-energy component of such a burst is barely detectable by GLAST. The internal optical depth of this set of parameters does not grow to very large values (maximum 10), so that the attenuation signature is not significant in Fig. 5(a). The dip around several 10^{13} eV corresponds to the optical depth peak, above which the attenuated flux starts to rise. The abrupt drop at several 10^{14} eV corresponds to the disappearance of the electron IC component at high energies.

10 CONCLUSIONS AND DISCUSSION

We have calculated the broad-band spectrum of GRBs from internal shocks for a wide range of parameter regimes. We did not take into account the external attenuation of TeV photons by the infrared radiation background and that of the PeV photons by the cosmic microwave background. These external processes would further attenuate our calculated spectrum in high-energy regimes, and reprocess the energy to delayed diffuse emission (Dai & Lu 2002; Stecker 2003; Razzaque et al. 2004; Wang et al. 2004; Casanova et al. 2007; Murase et al. 2007). Such processes are not relevant for most of the calculations presented, however, since the internal attenuation already cuts the observed spectrum below TeV. They are, however, important for high Lorentz factor cases in which more high-energy photons are leaked out of the internal shock region. The external attenuation is also prominant for high-energy emission from the external reverse/forward shocks and the external IC processes related to X-ray flares. These processes have been extensively discussed in other papers (referenced in Introduction) and they are not discussed in this paper. For nearby GRBs (e.g. $z < 0.3$), TeV emission is transparent. It is possible that ground-based Cherenkov detectors such as VERITAS, Milagro would detect TeV gamma rays from nearby energetic GRBs.

In previous treatments of hadronic components from internal shocks (Bhattacharjee & Gupta 2003; Fragile et al. 2004), the shock-accelerated protons are assumed to carry m_p/m_e times more energy than electrons. This effectively fixed $\epsilon_e \sim m_e/m_p$, which is not justified from the first principle. In this paper, we have taken all the equipartition parameters ϵ_e, ϵ_p and ϵ_B as free parameters, and explore the relative importance of various components in different parameter regimes. The dominant hadronic component emission becomes interesting only when ϵ_e is extremely small. Given the same observed level of sub-MeV spectrum, the total energy budget of the GRB needs to be very large.

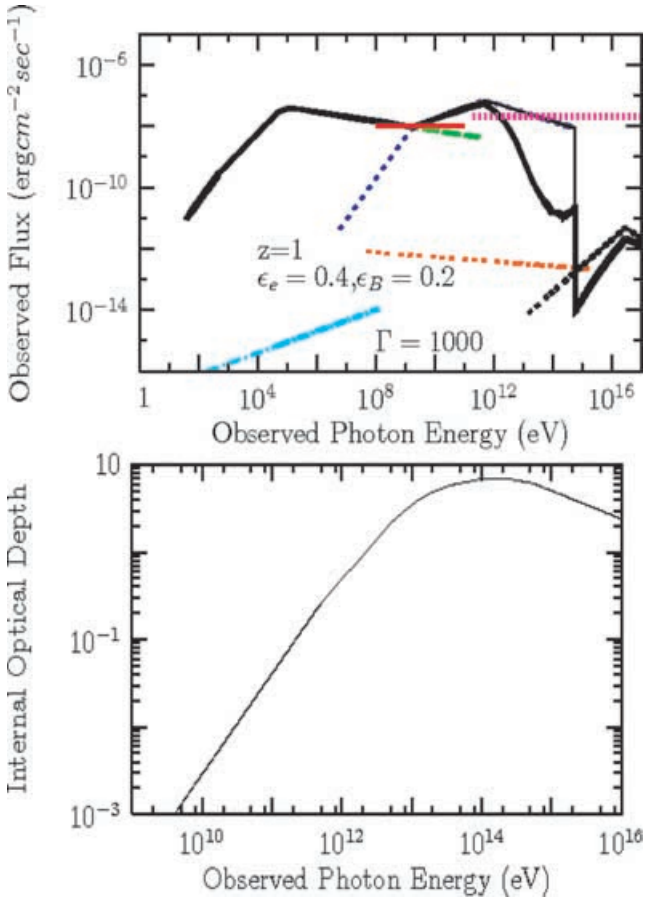

Figure 4. The case of a higher Lorentz factor. (a): The spectra of various components. Parameters: $\Gamma = 1000$ and $f_c = 50$. All the other parameters are the same as in Fig. 1. (b): The corresponding internal optical depths.

Inspecting the calculated spectra for different parameter sets (Figs 1–4), one finds that there is no clean picture to test the leptonic versus hadronic origin of the gamma rays. Such an issue may be, however, addressed by collecting both prompt and afterglow data. A moderate-to-high radiative efficiency would suggest a leptonic origin of high-energy photons, while a GRB with an extremely low radiative efficiency but an extended high-energy emission component would be consistent with (but not a proof for) the hadronic origin.

The prompt emission produced by leptons including the effect of pair production has been discussed by Pe'er & Waxman (2004), Pe'er et al. (2006). They calculated the emergent photon spectra for GRBs located at $z = 1$. The lower cut-off energy in the photon flux produced by leptons is determined by the synchrotron self-absorption energy, the minimum injection energy or the cooling energy depending on the values of the various GRB parameters. Our leptonic-component-dominated cases are consistent with their results, although we do not explore cases with very high compactness. If the electrons cool down to trans-relativistic energies, then their high-energy spectrum significantly deviates from broken power law (Pe'er et al. 2005, 2006). For our choice of values of the GRB parameters this effect is not important. Razzaque et al. (2004) estimated the internal optical depth for pair production and showed that at PeV energies the optical depth decreases with increasing photon energies. We have rederived the optical depths for values of GRB parameters. The results are generally consistent with that of Razzaque et al. (2004) except that the growth of optical depth with increasing energy is more gradual before the optical depth peak. This is a result of including the whole low-energy photon spectrum (rather than the threshold energy photons) for calculating the pair production optical depth. The optical depths depend on the cross-section of $\gamma\gamma$ interactions, the low-energy photon spectra, the various break energies in those spectra, luminosities, variability times and the GRB Lorentz factors. A change in values of any of these parameters may affect the values of the optical depths at various energies. For high bulk Lorentz factors, the π^0 component may appear in the final spectra due to the reduced optical depths around PeV energy. However, these ultrahigh-energy photons will be immediately absorbed in the GRB neighbourhood by cosmic microwave photons (Stecker 2003). The reradiated energy by the e^+e^- pairs would none the less contribute to the diffuse high-energy gamma-ray background (Casanova et al. 2007).

Upcoming gamma-ray detectors have a good chance of detecting prompt emission from GRBs and reveal their physical nature during the prompt phase. Detection of the hadronic components is difficult but it would be possible to infer the dominance of these components by a coordinated broadband observational campaign if they are indeed important. More generally, detection or non-detection of high-energy photons in the prompt phase would constrain the values of various GRB parameters. In particular, the pair attenuation feature would help to constrain the bulk Lorentz factor of the fireball. Compared with EGRET, GLAST has a 10 times larger collecting area and a larger field of

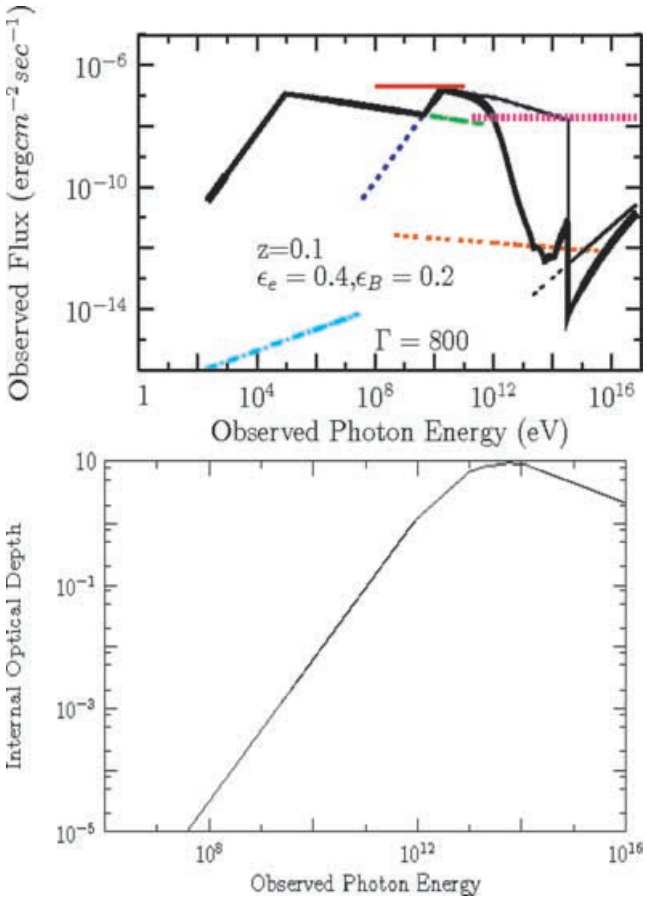

Figure 5. An energetic short GRB. (a): The spectra of various components. Parameters: $\epsilon_e = 0.4$, $\epsilon_B = 0.2$, $\epsilon_p = 0.4$, $t_v = 0.001$ s, $\Gamma = 800$, $f_c = 50$, $E_{iso} = 10^{51}$ erg and $L_{iso} = 10^{51}$ erg s^{-1}. The same line styles have been used as in Fig. 1. (b): The corresponding internal optical depths.

view. It is expected that GLAST LAT would detect high-energy emission from a large number of bursts (mostly long GRBs and some bright, relatively 'long' short GRBs), which will open a new era of studying GRBs in the GeV–TeV regime. On the other hand, it is difficult for VERITAS to detect prompt high-energy gamma rays even under the most optimistic conditions. High-energy emissions from the external shock at the early afterglow phase for nearby GRBs may be the better targets for VERITAS and other TeV detectors.

ACKNOWLEDGMENTS

We thank Brenda Dingus, Deirdre Horan, Enwei Liang, Peter Mészáros, Jay Norris, Asaf Pe'er, Soeb Razzaque, and Dave Thompson for useful discussion/comments and/or technical support. We also thank the anonymous referee for a detailed report with important suggestions and comments. This work is supported by NASA under grants NNG05GC22G, NNG06GH62G and NNX07AJ66G.

REFERENCES

Atkins R. et al., 2000, ApJ, 533, L119
Atkins R. et al., 2004, ApJ, 604, L25
Baring M. G., Harding A. K., 1997, ApJ, 491, 663
Barthelmy S. D. et al., 2005, Nat, 438, 994
Berestetskii V. B., Lifshitz E. M., Pitaevskii L. P., 1982, Quantum Electrodynamics. Pergamon, New York
Berger E. et al., 2005, Nat, 438, 988
Bhattacharjee P., Gupta N., 2003, Astropart. Phys., 20, 169
Bloom J. S. et al., 2006, ApJ, 638, 354
Burrows D. N. et al., 2005, Sci, 309, 1833
Bykov A., Mészáros P., 1996, ApJ, 461, L37
Casanova S., Dingus B., Zhang B., 2007, ApJ, 656, 306
Chiang J., Dermer C. D., 1999, ApJ, 512, 699
Dai Z. G., Lu T., 2002, ApJ, 580, 1013
Dermer C. D., 2007, ApJ, submitted (astro-ph/0703223)
Dermer C. D., Bottcher M., Chiang J., 2000a, ApJ, 537, 255

Dermer C. D., Chiang J., Mitman K. E., 2000b, ApJ, 537, 785
Fan Y. Z., Piran T., 2006, MNRAS, 370, L24
Fan Y. Z., Zhang B., Wei D. M., 2005, ApJ 628, L25
Fan Y.-Z., Piran T., Narayan R., Wei D.-M. 2007, MNARS, submitted (asXiv:0704.2063)
Fox D. B. et al., 2005, Nat, 437, 845
Fragile P. C., Mathews G. J., Poirier J., Totani T., 2004, Astropart. Phys., 20, 591
Gehrels N. et al., 2005, Nat, 437, 851
Gehrels N., Michelson P., 1999, Astropart. Phys., 11, 277
Ghisellini G., Celotti A., Lazzati D., 2000, MNRAS, 313, L1
Gonzalez M. M., Dingus B. L., Kaneko Y., Preece R. D., Dermer C. D., Briggs M. S., 2003, Nat, 424, 749
Gould R. J., Schreder G. P., 1967, Phys. Rev., 155, 1404
Gou L. J., Mészáros P. 2007, ApJ, submitted (asXiv:0705.1545)
Granot J., Sari R., 2002, ApJ, 568, 820
Gupta N., Zhang B., 2007, Astropart. Phys., 27, 386
Horan D. et al., 2007, ApJ, 655, 396
Hurley K. et al., 1994, Nat, 372, 652
Jauch J. M., Rohrlich F., 1955, The Theory of Photons and Electrons. Addison-Wesley
Jones B. B. et al., 1996, ApJ, 463, 565
Lemoine M., Pelletier G., 2003, ApJ, 589, L73
Li Z., Song L. M., 2004, ApJ, 608, L17
Lithwick Y., Sari R., 2001, ApJ, 555, 540
Longo F., Cocco V., Tavani M., 2002, Nucl. Inst. Meth. A, 486, 610
Mészáros P., 2006, Rep. Prog. Phys., 69, 2259
Mészáros P., Rees M. J., 1994, MNRAS, 269, L41
Mészáros P., Rees M. J., Papathanassiou H., 1994, 432, 181
Molinari E. et al., 2007, A&A, 469, L13
Mundell C. G. et al., 2007, ApJ, 660, 489
Murase K., Asano K., Nagataki S., 2007, ApJ, submitted (astro-ph/0703759)
Panaitescu A., Mészáros P., 1998, ApJ, 501, 772
Panaitescu A., Kumar P., 2000, ApJ, 543, 66
Panaitescu A., Kumar P., 2002, ApJ, 571, 779
Pilla R. P., Loeb A., 1998, ApJ, 494, L167
Pe'er A., Waxman E., 2004, ApJ, 613, 448
Pe'er A., Waxman E., 2005, ApJ, 633, 1018; Erratum-ibid., 2006, 638, 1187
Pe'er A., Mészáros P., Rees M. J., 2005, ApJ, 635, 476
Pe'er A., Mészáros P., Rees M. J., 2006, ApJ, 642, 995
Pe'er A., Zhang B., 2006, ApJ, 653, 454
Rachen J. P., Mészáros P., 1998, Phys. Rev. D, 58, 123005
Razzaque S., Zhang B., 2007, in preparation
Razzaque S., Mészáros P., Zhang B., 2004, ApJ, 613, 1072
Rees M. J., Mészáros P., 1994, ApJ, 430, L93
Rybicki G., Lightman A. P., 1979, Radiative Processes in Astrophysics. Wiley, New York
Sari R., Esin A., 2001, ApJ, 548, 787
Sari R., Piran T., Narayan R., 1998, ApJ, 497, L17
Schady P. et al., 2007, MNRAS, submitted (astro-ph/0611081)
Stecker F., 2003, J. Phys. G, 29, R47
Totani T., 1998, ApJ, 509, L81
Vietri M., 1997, Phys. Rev. Lett., 78, 4328
Villasenor J. S. et al., 2005, Nat, 437, 855
Wang X. Y., Cheng K. S., Dai Z. G., Lu T., 2004, ApJ, 604, 306
Wang X. Y., Dai Z. G., Lu T., 2001a, ApJ, 546, L33
Wang X. Y., Dai Z. G., Lu T., 2001b, ApJ, 556, 1010
Wang X.-Y., Li Z., Mészáros P., 2006, ApJ, 641, L89
Waxman E., 1995, Phys. Rev. Lett., 75, 386
Waxman E., Bahcall J., 1997, Phys. Rev. Lett., 78, 2292
Wei D. M., Lu T., 1998, ApJ, 505, 252
Zhang B., 2007, Chinese J. Astron. &Astrophys., 7, 1
Zhang B., Mészáros P., 2001, ApJ, 559, 110
Zhang B., Mészáros P., 2002, ApJ, 581, 1236
Zhang B., Fan Y. Z., Dyks J., Kobayashi S., Mészáros P., Burrows D. N., Nousek N., Gehrels N., 2006, ApJ, 642, 354
Zhang B. et al., 2007, ApJ, 655, 989

This paper has been typeset from a TEX/LATEX file prepared by the author.